ELSEVIER

Journal of Power Sources 106 (2002) 264–273

JOURNAL OF POWER SOURCES

www.elsevier.com/locate/jpowsour

Steam reforming of methanol over copper-based monoliths: the effects of zirconia doping

Bård Lindström, Lars J. Pettersson*

KTH-Royal Institute of Technology, Department of Chemical Engineering and Technology, Chemical Technology, (SE-100 44) Stockholm, Sweden

Abstract

In this paper, an experimental investigation concerning steam reforming of methanol over various alumina-supported monolithic copper-based catalysts is presented. The activity and carbon dioxide selectivity was studied over two sets of catalysts, one of which was doped with zirconium, with five different copper contents. The zirconium-doped catalyst were less active with respect to the hydrogen yield, however, they were at all times more selective towards carbon dioxide over the entire temperature interval. The catalysts have been characterised using Brunauer–Emmett–Teller (BET) surface area measurement and X-ray diffraction (XRD). The results show that the copper loading and modification of the active material by zirconia doping had a great influence on the methanol conversion and carbon dioxide selectivity of the steam reforming reaction.

Keywords: Monolith; Fuel cell; Automotive applications; Steam reforming; Methanol

1. Introduction

1.1. Automotive fuel cell applications

The fuel cell vehicle has a high potential to fulfil the long-term objective of zero-emission vehicles, as proposed by the California Environmental Protection Agency's Air Resources Board (ARB). The sensitivity of the fuel cell for poisons, such as carbon monoxide (CO), is a severe constraint for introducing the technology in automotive applications. CO concentrations above 50 ppm can lower the performance of a polymer electrolyte fuel cell (PEFC) system considerably [1]. Providing the almost CO-free hydrogen required by the fuel cell to generate electricity is a challenging task associated with automotive fuel cell applications.

The existing distribution system for motor fuels is almost solely based on liquid fuels. Hydrogen can either be stored or be produced on-board from a liquid fuel with high hydrogen content. Pure hydrogen can be stored either as a gas at high pressures or in liquid phase at $-253\,^{\circ}C$. Hydrogen storage as metal hydrides is currently being developed as storage solution. The cost of revamping the gasoline tanks to operate with an alternative liquid fuel is considerably lower than for a pressurized or liquefied gas.

Catalytic conversion of liquids with high hydrogen to carbon ratio, such as primary alcohols, is possible at relatively low temperatures (200–300 °C) and sought of by the automotive industry as one of the most promising solutions for generating the hydrogen on-board the vehicle [2]. Methanol is today a primary candidate as hydrogen carrier for the on-board production of hydrogen, due to its high hydrogen to carbon ratio (4:1), low boiling point and high availability. The absence of carbon–carbon bonds in methanol drastically reduces the risk of coking. Methanol is today produced as a large-scale commodity chemical with a world-wide production capacity exceeding 33 million metric tonnes. Most of the methanol in the world is produced from natural gas, but methanol can also be produced from renewable resources and, thus lowering the production of greenhouse gases.

1.2. The methanol reforming process

Decomposition, partial oxidation and steam reforming are the three most important processes to produce hydrogen from methanol [3]. Thermal or catalytic decomposition Eq. (1) is the most simple process from a chemical standpoint as solely methanol is used as feedstock [4].

$$CH_3OH(g) \rightarrow 2H_2 + CO \quad \Delta H^0 = 91\,kJ/mol \tag{1}$$

The decomposition of methanol yields a product gas containing up to 67% hydrogen and 33% carbon monoxide. Although, highly useful as fuel for internal combustion

* Corresponding author. Tel.: +46-8-790-8259; fax: +46-8-10-8579.
E-mail address: larsp@ket.kth.se (L.J. Pettersson).

0378-7753/02/$ – see front matter
PII: S0378-7753(01)01016-3

engines [4], this gas mixture puts excessive demands on the CO clean-up system if it would be used as fuel for a PEFC. Furthermore, the highly endothermic nature of the process can cause limitations in automotive applications where energy supply is scarce.

Partial oxidation Eq. (2) is a fast and exothermic reaction, which has caught on a considerable interest in the research community [5–7]. By using this process, it is possible to design compact and highly responsive systems. It is possible to achieve a product stream with hydrogen concentrations up to 67% if methanol is partially oxidised with pure oxygen in the feed. However, for automotive solutions the required oxygen would most likely be supplied from air, diluting the product gas with nitrogen. In such a system the maximum theoretical hydrogen content is lowered to 41%. The hydrogen concentration is directly linked to the fuel cell's ability to utilize the incoming hydrogen. At low concentrations mass transfer limits the reaction rate and, thus the amount of hydrogen converted to electricity is lowered [8].

$$CH_3OH(g) + \tfrac{1}{2}O_2 \rightarrow 2H_2 + CO_2 \quad \Delta H^0 = -192\,\mathrm{kJ/mol} \tag{2}$$

Caution must be taken during reactor design, because of the highly exothermic nature of the partial oxidation process. Hot spots can be formed in the reactor, which can cause catalyst deactivation of the reforming catalyst through sintering and thereby increased particle growth. As a result, the performance of the vehicle will deteriorate.

Steam reforming is a highly efficient conversion process Eq. (3), which has received much attention [9–11] due to the ability to produce a gas with high hydrogen concentration (75%) while maintaining a high carbon dioxide selectivity. The main drawback of steam reforming is that the reaction is moderately endothermic. The use of surplus heat from the effluent of the catalytic burner could satisfy the energy demand (see Fig. 1).

$$CH_3OH(g) + H_2O(g) \rightarrow 3H_2 + CO_2 \quad \Delta H^0 = 50\,\mathrm{kJ/mol} \tag{3}$$

The steam reforming process is usually operated with excess steam, to induce the Water gas shift (WGS) reaction Eq. (4) in the reformer in order to lower the CO concentration in the product gas.

$$CO + H_2O(g) \rightarrow H_2 + CO_2 \quad \Delta H^0 = -41\,\mathrm{kJ/mol} \tag{4}$$

The WGS reaction reduces the carbon monoxide content while increasing the hydrogen content in the product stream. At equilibrium conditions the forward reaction is favoured by low temperatures [12]. It is important to have an efficient reformer including a WGS step, since, this reduces the volume of the subsequent CO removal step.

The CO clean-up unit usually consists of a multi-bed configuration with inter-stage cooling. The CO conversion is performed using selective oxidation with air over a supported platinum catalyst [13]. The CO removal unit requires a large volume, which is not available in modern automobiles. Furthermore, the clean-up process decreases the efficiency of the fuel cell system, since, considerable amounts of hydrogen is consumed.

This study is focused on the steam reforming reaction due to the superiority of the process with respect to methanol conversion and carbon dioxide selectivity.

1.3. Monoliths as catalyst substrates in automotive reformers

Monoliths are uniform extruded structures composed of parallel flow-through channels and are usually based upon ceramic materials or aluminium-containing metals (see Fig. 2). Monoliths as catalyst substrates had their breakthrough when exhaust gas catalysts were introduced on a large scale in the USA [14]. In the beginning of the 1980's, the automotive industry most commonly used fixed-bed reactors with pellets [15], but these were phased out when the monolith technology was starting to mature and large-scale production was possible. Ceramic monoliths are usually made of cordierite, a magnesium aluminium silicate mineral, which is substantially more robust than their pellet counterparts. The biggest problem with using pellets, apart from the high pressure drops in catalytic fixed-bed reactors, is pellet attrition and thermal degradation. In an automotive application chassis vibrations and road shocks are inevitable. Using metallic reactors filled with catalyst pellets at high temperatures means that the reactor walls will expand more than the bed and the reactor volume will increase somewhat, due to the big difference in thermal conductivity.

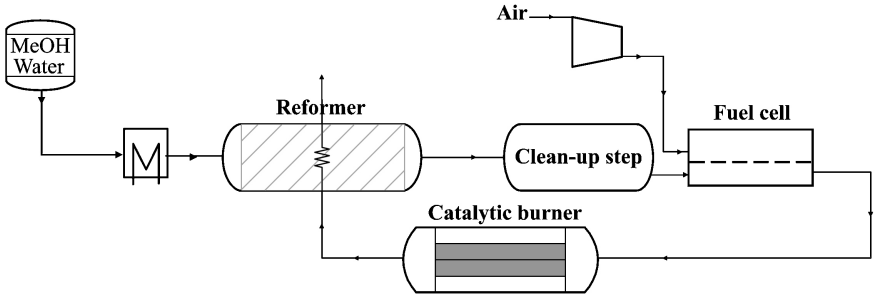

Fig. 1. Methanol reforming system.

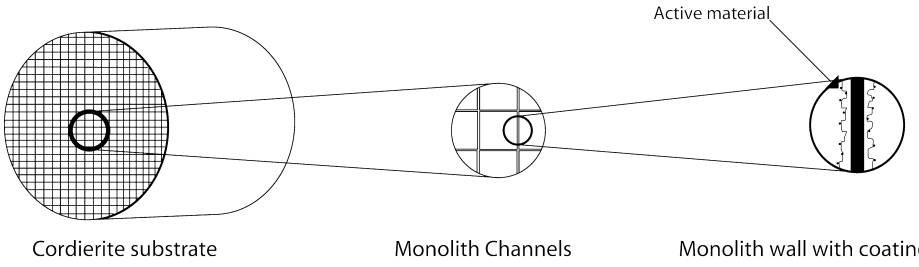

Fig. 2. Schematic view of a monolith.

When the reactor is cooled it will return to its original volume and some of the pellets will be crushed and the catalyst will lose activity. For methanol reforming this is a minor problem compared to reforming of gasoline or diesel, which require considerably higher temperatures.

The ceramic catalyst substrates offer the advantages of high surface-to-volume ratio, large open frontal area, low thermal mass, low heat capacity, low thermal expansion, high strength and high temperature of operation [16]. These factors will improve quick light-off, increase conversion, decrease pressure drop and improve both thermal and mechanical shock resistance. On the other hand, one obvious disadvantage with monolithic catalysts is their lower content of active material per unit reactor volume. Besides, the flow characteristics are not favourable in a monolith. The Reynold's number will decrease substantially in a monolith channel compared to in a fixed-bed. Consequently, due to the laminar flow both heat and mass transfer characteristics are influenced in a negative way. There is no mass transfer in the radial direction between channels, which decreases the conversion. Some of these drawbacks can be addressed by using, for example segmented monoliths. Taking this into account it is important to prepare the catalyst in such a way that the active phase is highly active [17]. A high loading, a high dispersion and a uniform active phase distribution are desired. The ceramic substrate used in automotive catalysts is coated with a high surface area inorganic oxide, i.e. γ-Al_2O_3, upon which the active material is dispersed [18]. For endothermic reactions, such as steam reforming, the use of monoliths can be problematic as heat transfer is poor between the channels, due to the low heat conductivity of the ceramic material.

In these experiments, we have chosen copper-based materials, as they were highly active in previous tests using pellets [19], for investigating the feasibility of using monoliths for automotive reforming.

2. Experimental

2.1. Catalyst preparation

The cordierite ($2MgO{\cdot}5SiO_2{\cdot}2Al_2O_3$) monolith substrate was initially coated with aluminium oxide (γ-Al_2O_3), to increase the surface area and to enable dispersion of the catalytic material. The γ-Al_2O_3 powder (see Table 1 for material data) was suspended in ethanol and ball milled for 24 h prior to coating the monolith. The monolith was then dipped into the γ-Al_2O_3 slurry and dried for 1 h at 120 °C. The procedure was repeated until 15 wt.% γ-Al_2O_3 had been deposited on the monolith.

The active materials (see Table 2), all in the form of nitrates, were dissolved in water and the pH kept above the iso-electric point of γ-Al_2O_3. The metal salts were mixed in fixed weight ratios (see Table 2) and the γ-Al_2O_3 coated monoliths were dipped in the metal nitrate solutions. The monoliths were then dried at 120 °C for 2 h and calcined at 350 °C for 5 h. The total metal loading of each monolith was 15 wt.% of the washcoat. The zirconium-doped catalysts were loaded with 10 wt.% zirconium of the total metal loading.

In order to differentiate between the catalyst containing only copper and zinc and those doped with zirconia, the following notation is used: Cu/Zn for the catalysts containing only copper and zinc and Cu/Zn [Zr] for those doped. The numerical values indicate the mass distribution between Cu and Zn.

Table 1
Material data

Material	Data	Manufacturer
Ethanol (C_2H_5OH)	99.5 vol.% spectroscopic	Kemetyl
Alumina (γ-Al_2O_3)	Surface area 150 g/m^2	Condea
Monolith	Cordierite 400 cpsi	Corning
$Cu(NO_3)_2{\cdot}xH_2O$	M_w: 241.5 g/mol	Alfa Aesar
$Zn(NO_3)_2{\cdot}xH_2O$	M_w: 297 g/mol	Merck
$ZrO(NO_3)_2{\cdot}xH_2O$	M_w 231.2 g/mol	Alfa Aesar

Table 2
Catalyst composition

Catalyst Cu/Zn	Active material (wt.%)	Catalyst Cu/Zn [Zr]	Active material (wt.%)
100/0	15.3	100/0	15.3
80/20	14.9	80/20	15.2
60/40	15.2	60/40	15.3
40/60	15.3	40/60	15.2
20/80	15.2	20/80	15.2
0/100	15.4		

2.2. Catalyst activity

The catalytic material was tested in a tubular reactor operating at atmospheric pressure. The reactants were fed to the reactor with 30% excess steam in order to lower CO concentrations by inducing the WGS reaction.

Prior to each experiment the catalyst was reduced in a 10% H_2 in N_2 mixture at a heating rate of 5 °C/min and dwelling at 220 °C for 2 h. The product stream composition was measured on-line using a gas chromatograph from Varian equipped with both TCD and FID detectors. The experiments were carried out over a temperature interval of 200–300 °C, where the temperature is measured outside the axial entrance of the monolith. The methanol/steam mixture was preheated to the reactor temperature in order to compensate for the limitations in heat transfer in the cordierite monolith [20]. The reactor was made of stainless steel (ASTM 316) with an inner diameter of 25 mm. For all experiments a space velocity (SV) of 10,000 h^{-1} was used. Three monoliths of the following size were used in series: 22 mm in diameter and 20 mm in length. A detailed schematic of the laboratory test system is presented in Fig. 3.

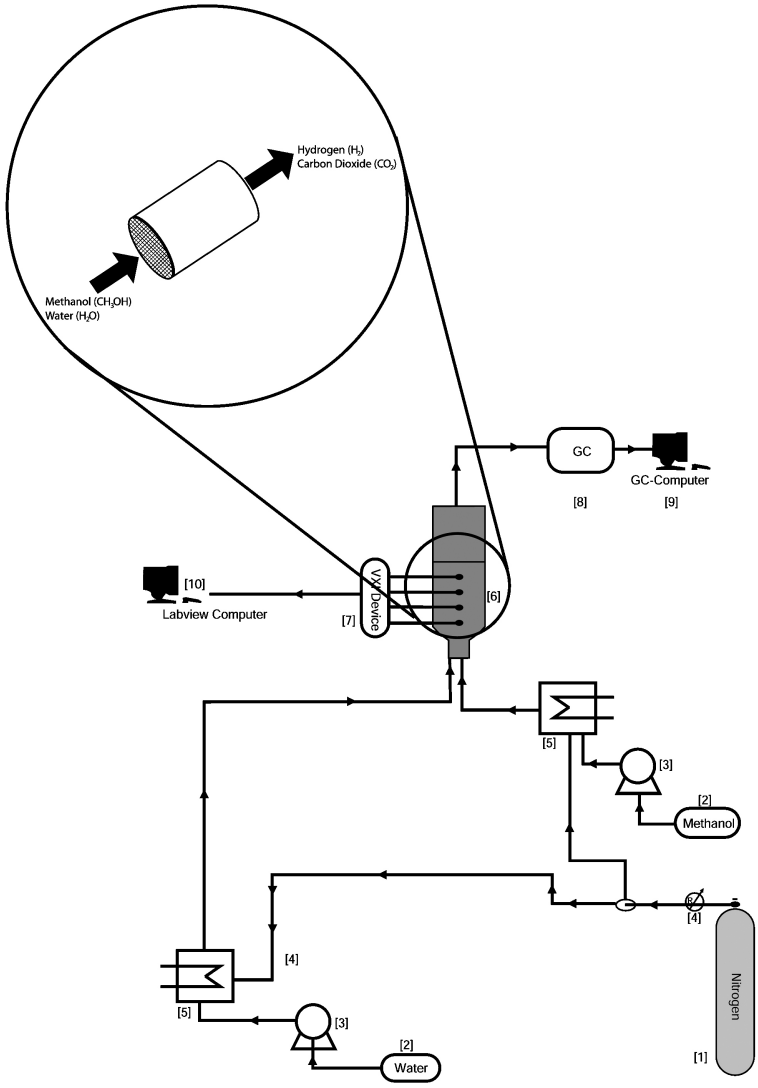

Equipment Description

1:Carrier gas (99.999 % Nitrogen AGA)	6 :Flow reactor
2:Fuel Tanks (Deionized water and 99.9 % Methanol)	7 :Thermocouple module (National Instruments)
3:Pumps (Braun Perfusor)	8 :Varian Gas Chromatograph (FID & TCD detectors)
4:Mass flow controller (Bronkhorst HI-TEC)	9 :Computer with GC evaluation software
5:Evaporators	10:Computer with Labview for temperature measurement

Fig. 3. Laboratory reactor system.

2.3. X-ray diffraction

The crystal phases were identified by means of X-ray powder diffraction (XRD) using a Siemens Diffraktometer 5000. The operating parameters were: monochromatic Cu-Kα radiation, Ni filter, 30 mA, 40 kV, 2θ scanning from 10 to 90°, and a scan step-size 0.02. Phase identification was done using the reference database (JCPDS-files) supplied with the equipment.

2.4. BET surface area measurements

The specific surface area of the various samples was measured according to the Brunauer–Emmett–Teller theory (BET) by nitrogen adsorption using a Micrometrics ASAP 2010 instrument. Prior to adsorption measurements, the samples were degassed for at least 12 h at 220 °C.

3. Results

3.1. Catalyst activity measurements

The catalysts were tested using the steam reforming process. For details on the catalyst make-up consult the section on experimental work. The results are presented as volumetric concentrations of hydrogen (H_2), carbon dioxide (CO_2), carbon monoxide (CO) and CO_2 selectivity (S_e). The equation used to derive the CO_2 selectivity (S_e) is described in Eq. (5). All concentrations presented in this paper have been compensated for the presence of inert nitrogen and excess steam.

$$S_e(\%) = \frac{(CO_2)}{(CO_2 + CO)} \times 100 \quad (5)$$

The results show that CO was the main by-product formed in the reforming process. This agrees well with the reaction mechanisms proposed by Amphlett and co-workers [9,11].

The effect of varying the copper loading for the Cu/Zn catalysts is shown in Fig. 4a and b. The highest hydrogen yield was obtained by the Cu60/Zn40 catalyst with hydrogen concentrations close to the theoretical maximum of 75% at temperatures above 250 °C. The lowest hydrogen yield was observed by the catalyst with no copper loading (Zn100). The catalyst with 20 wt.% copper loading (Cu20/Zn80) exhibited a considerably lower activity compared to the other catalysts at temperatures below 250 °C. The CO_2 selectivity was above 94% for all of the catalysts, with the exception of the Cu20/Zn80 and Zn100 catalysts which generated slightly lower CO_2 selectivity than the other Cu/Zn catalysts at temperatures above 240 °C. For temperatures below 220 °C the CO_2 selectivity for the Cu20/Zn80 and

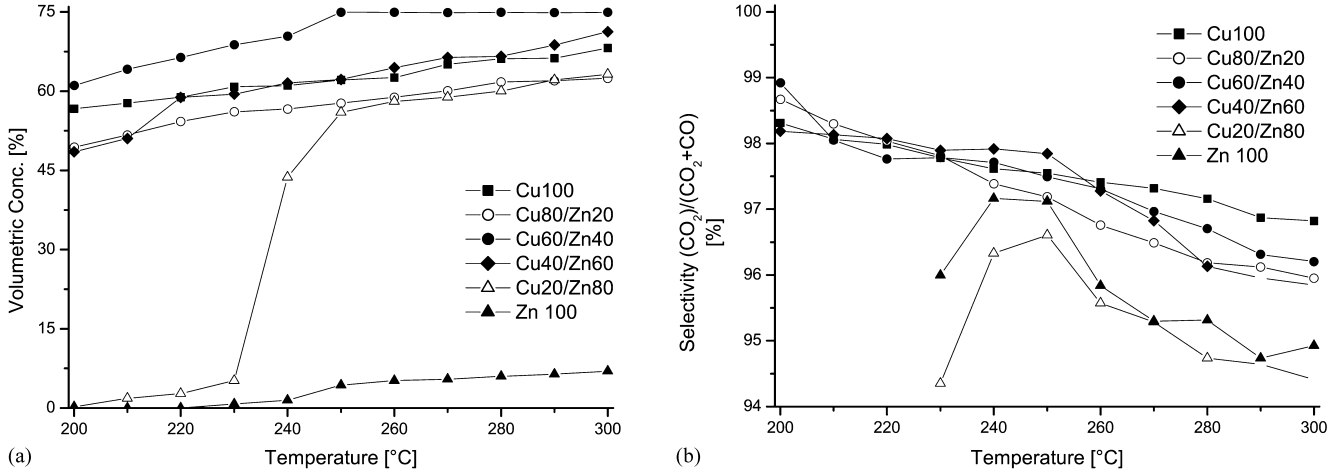

Fig. 4. (a) Hydrogen concentration; (b) carbon dioxide selectivity.

Table 3
Impact of variations of copper content

Catalyst	H_2 210 °C (vol.%)	H_2 max (vol.%)	T 60% H_2 (°C)	S_e min (%)[a]	S_e mean (%)[a]	CO max (vol.%)
Cu100	58	68	225	97	98	0.69
Cu80/Zn20	52	62	269	96	97	0.85
Cu60/Zn40	64	75	195	96	97	0.96
Cu40/Zn60	51	71	238	96	97	1.0
Cu20/Zn80	1.8	63	279	0	80	1.2
Zn100	–	6.9	–	0	96	0.12

[a] S_e: carbon dioxide selectivity.

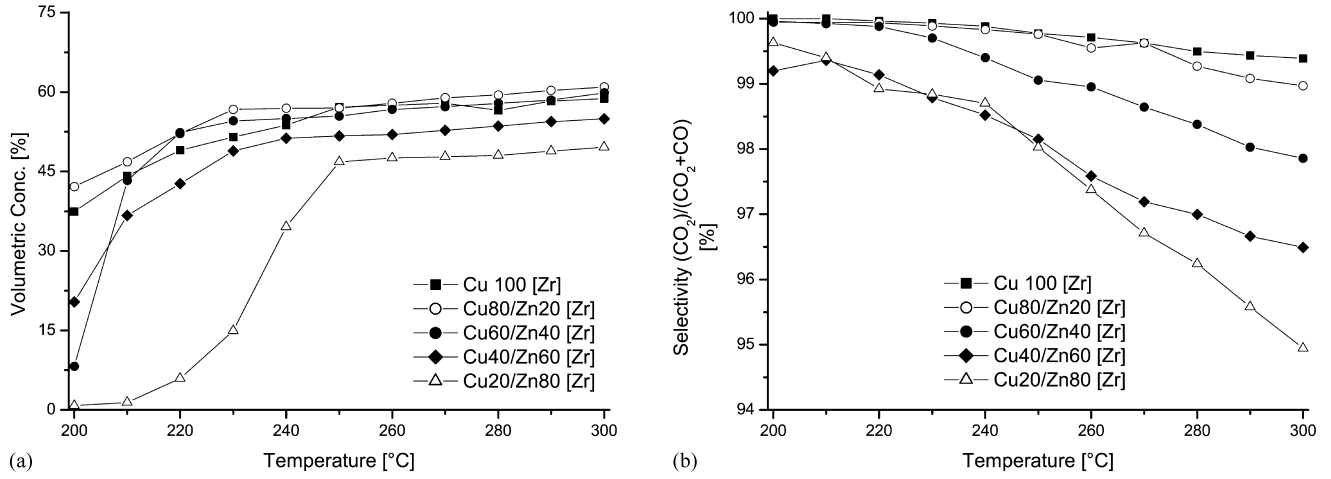

Fig. 5. (a) Hydrogen concentration; (b) carbon dioxide selectivity.

Zn100 catalysts was close to zero. The results are summarised in Table 3.

The effect of varying the copper loading for the Zr-doped catalysts is shown in Fig. 5a and b. The impact of the copper content on the performance of the catalysts is lower for the Zr-doped catalysts compared to the Cu/Zn catalysts. The Cu80/Zn20 [Zr] catalyst generated the highest hydrogen yields. The performance of the Cu100 [Zr] and Cu60/Zn40 [Zr] catalysts were near to that of the Cu80/Zn20 [Zr] catalysts. The CO_2 selectivity followed the same trend as the activity with the Cu100 [Zr] catalyst having the highest CO_2 selectivity closely followed by the Cu80/Zn20 [Zr] and Cu60/Zn40 [Zr] catalysts. The results of the Zr-doped catalysts are summarised in Table 4.

A comparison between the Cu100 and Cu100 [Zr] catalysts is shown in Fig. 6a and b. The Cu100 had a higher activity at all temperatures compared to the Cu100 [Zr], with hydrogen concentrations above 65%. The trend of the CO_2 selectivity was the reverse of the activity. The Zr-doped catalyst was superior compared to the Cu100 catalyst, with a CO_2 selectivity above 99% for the entire temperature interval. The CO_2 selectivity for the Cu100 catalyst was above 96% for the whole operating window.

In Fig. 7a and b the activity and CO_2 selectivity for the Cu80/Zn20 and Cu80/Zn20 [Zr] is presented. The activity for the two catalysts is comparable with the Cu80/Zn20 yielding a slightly higher hydrogen concentration at temperatures above 260 °C. For both catalysts, hydrogen concentrations over 60% are obtained only at temperatures above 270 °C. The CO_2 selectivity for the Zr-doped catalyst is again much higher with a CO_2 selectivity above 99% for the entire temperature interval. The CO_2 selectivity for the Cu/Zn catalyst was above 95% for the whole temperature span.

The hydrogen yields for the Cu60/Zn40 and Cu60/Zn40 [Zr] catalysts are shown in Fig. 8a. The Cu/Zn catalyst had a higher hydrogen concentration for the entire temperature interval. Reforming over the Cu/Zn catalyst generated a hydrogen concentration above 70% at temperatures over 250 °C. The CO_2 selectivity, see Fig. 8b, followed the reverse trend with the Cu/Zn [Zr] catalyst having a relatively higher CO_2 selectivity than the Cu/Zn catalyst. The CO_2 selectivity for the Cu/Zn [Zr] catalyst was above 98% for all temperatures, whereas, the Cu/Zn catalyst had a CO_2 selectivity above 96% for the whole interval.

For the Cu40/Zn60 and Cu40/Zn60 [Zr] catalyst the hydrogen yields (see Fig. 9a) were higher for the Cu/Zn catalyst compared to the Cu/Zn [Zr] catalyst at all temperatures. The difference in hydrogen concentrations for the catalysts was relatively constant over the entire temperature span. The Cu/Zn [Zr] catalyst yielded hydrogen concentrations below 50% at all temperatures. The Cu/Zn catalyst produced hydrogen concentrations above 70% at 280 °C. The CO_2 selectivity (Fig. 9b) were higher for the Cu/Zn [Zr] catalyst, however, the gap in performance, with respect to the selectivity, between the catalysts was lower compared to

Table 4
Impact of variations of copper content on Zr-doped catalysts

Catalyst	H_2 210 °C (vol.%)	H_2 max (vol.%)	T 60% H_2 (°C)	S_e min (%)[a]	S_e mean (%)[a]	CO max (vol.%)
Cu100 [Zr]	44	59	–	99	100	0.12
Cu80/Zn20 [Zr]	47	61	285	99	100	0.21
Cu60/Zn40 [Zr]	43	60	–	98	99	0.43
Cu40/Zn60 [Zr]	37	55	–	97	98	0.65
Cu20/Zn80 [Zr]	1.4	50	–	95	98	0.85

[a] S_e: carbon dioxide selectivity

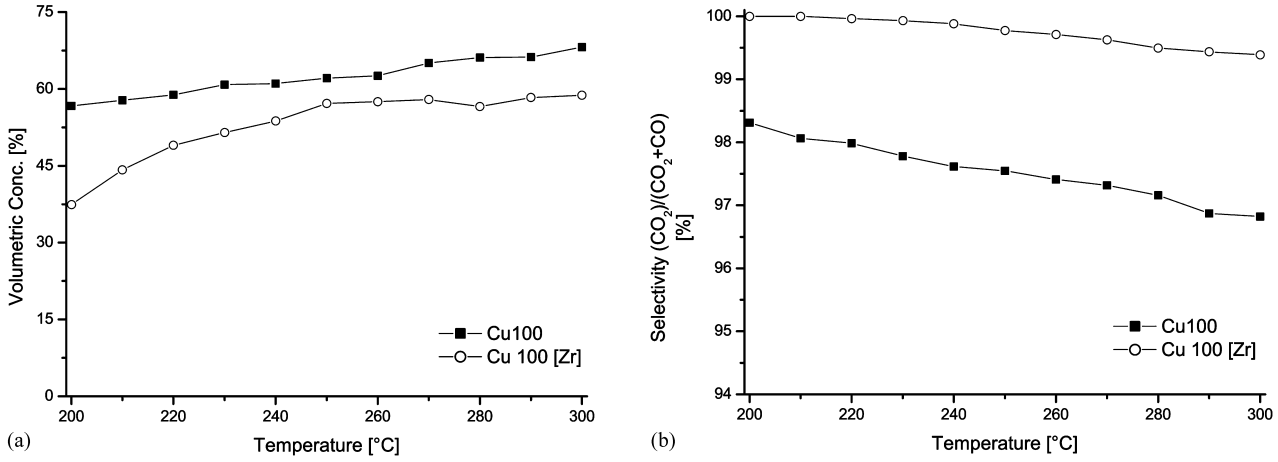

Fig. 6. (a) Hydrogen concentration; (b) carbon dioxide selectivity.

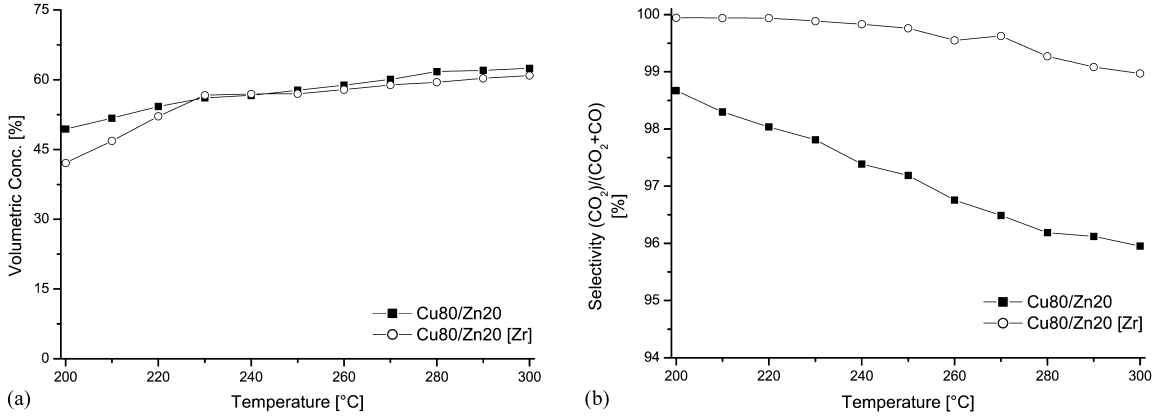

Fig. 7. (a) Hydrogen concentration; (b) carbon dioxide selectivity.

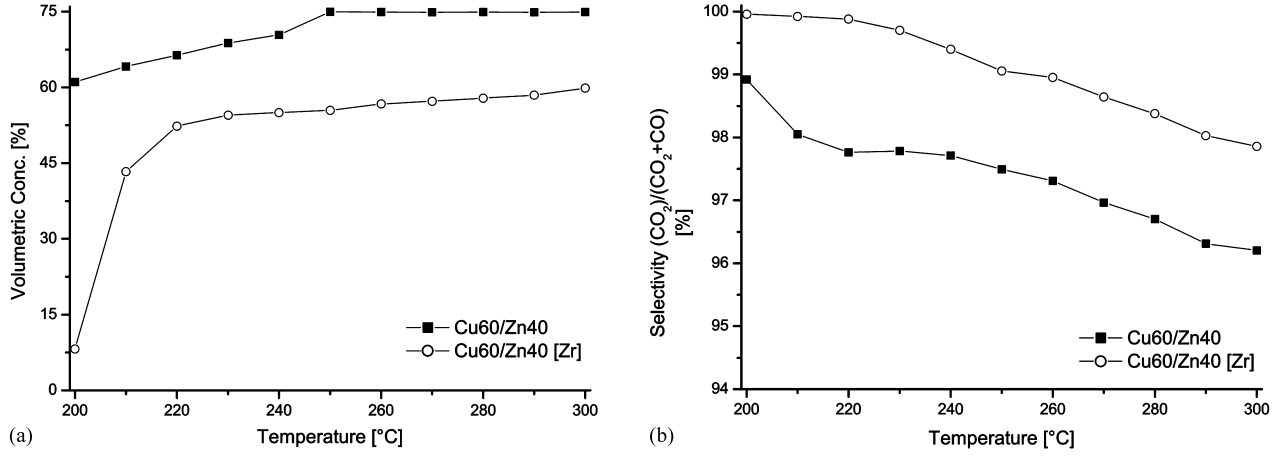

Fig. 8. (a) Hydrogen concentration; (b) carbon dioxide selectivity.

the other catalysts in the experiments. The selectivity was above 96% for both catalysts.

Fig. 10a and b shows the activity and selectivity for the Cu20/Zn80 and Cu20/Zn80 [Zr] catalysts. The activity for both catalysts is low at temperatures below 240 °C. The Cu/Zn catalyst exhibits lower activity than the Cu/Zn [Zr] catalyst at temperatures below 230 °C, however, at higher temperatures the Cu/Zn catalyst is superior with respect to

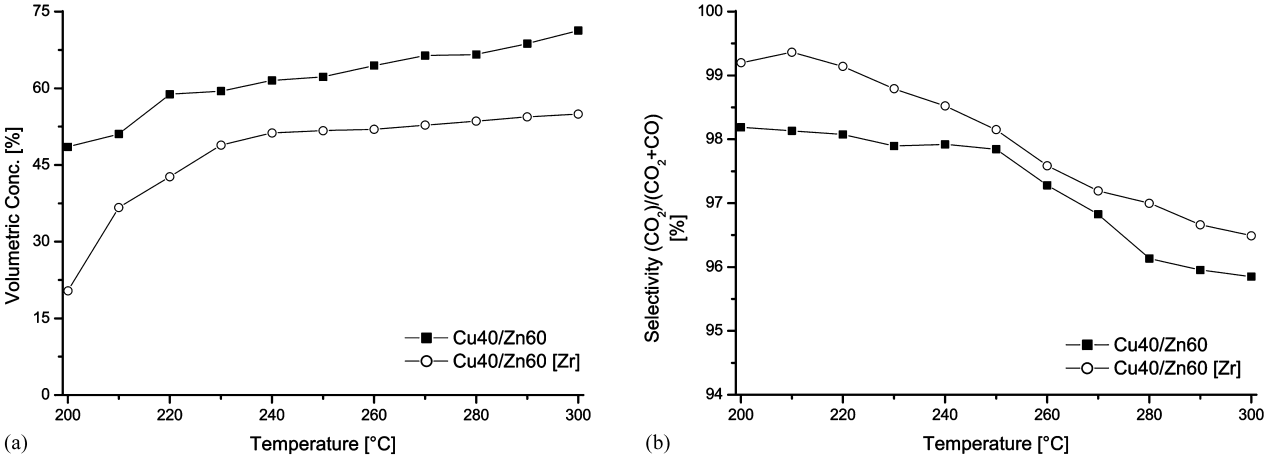

Fig. 9. (a) Hydrogen concentration; (b) carbon dioxide selectivity.

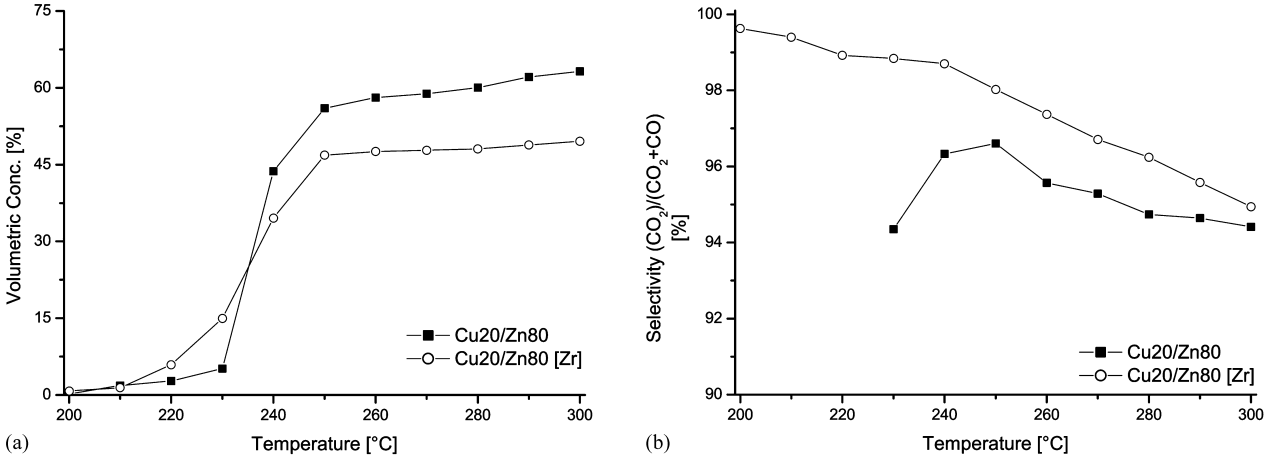

Fig. 10. (a) Hydrogen concentration; (b) carbon dioxide selectivity.

the hydrogen yields. The CO_2 selectivity is higher for the Cu/Zn [Zr] catalyst at all temperatures with selectivity above 95% for the entire temperature interval. For temperatures below 220 °C the CO_2 selectivity for the Cu20/Zn80 catalyst was close to zero. The results of the material comparison is summarised in Table 5.

3.2. Characterisation

Figs. 11 and 12 show the X-ray diffractograms obtained for the Cu/Zn and Cu/Zn [Zr] catalysts, respectively. The XRD spectra were collected after calcination at 350 °C and reduction in 10% H_2 in N_2 at 220 °C for 2 h. The copper was

Table 5
Effect of zirconium doping

Catalyst	H_2 210°C (vol.%)	H_2 max (vol.%)	T 60% H_2 (°C)	S_e min (%)[a]	S_e mean (%)[a]	CO max (vol.%)
Cu100	58	68	225	97	98	0.69
Cu100 [Zr]	44	59	–	99	100	0.12
Cu80/Zn20	52	62	269	96	97	0.85
Cu80/Zn20 [Zr]	47	61	285	99	100	0.21
Cu60/Zn40	64	75	195	96	97	0.96
Cu60/Zn40 [Zr]	43	60	–	98	99	0.43
Cu40/Zn60	51	71	238	96	97	1.0
Cu40/Zn60 [Zr]	37	55	–	97	98	0.65
Cu20/Zn80	1.8	63	279	0	80	1.2
Cu20/Zn80 [Zr]	1.4	50	–	95	98	0.85

[a] S_e: carbon dioxide selectivity.

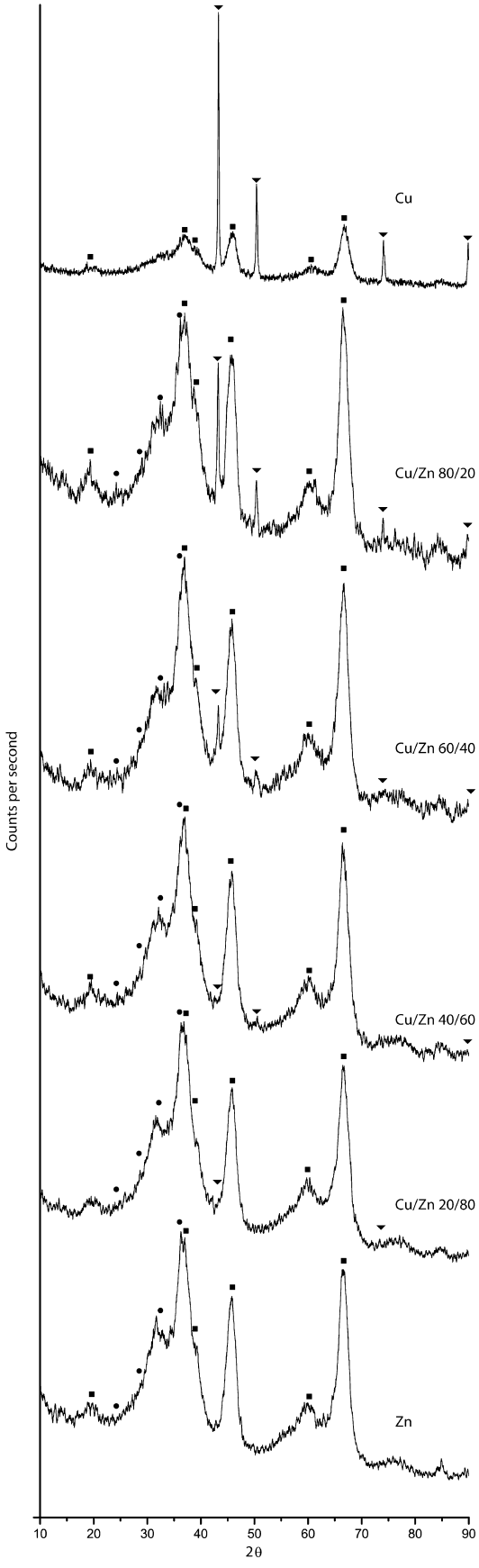

Fig. 11. X-ray diffraction spectra. Cu (▼), γ-Al_2O_3 (■), ZnO (●).

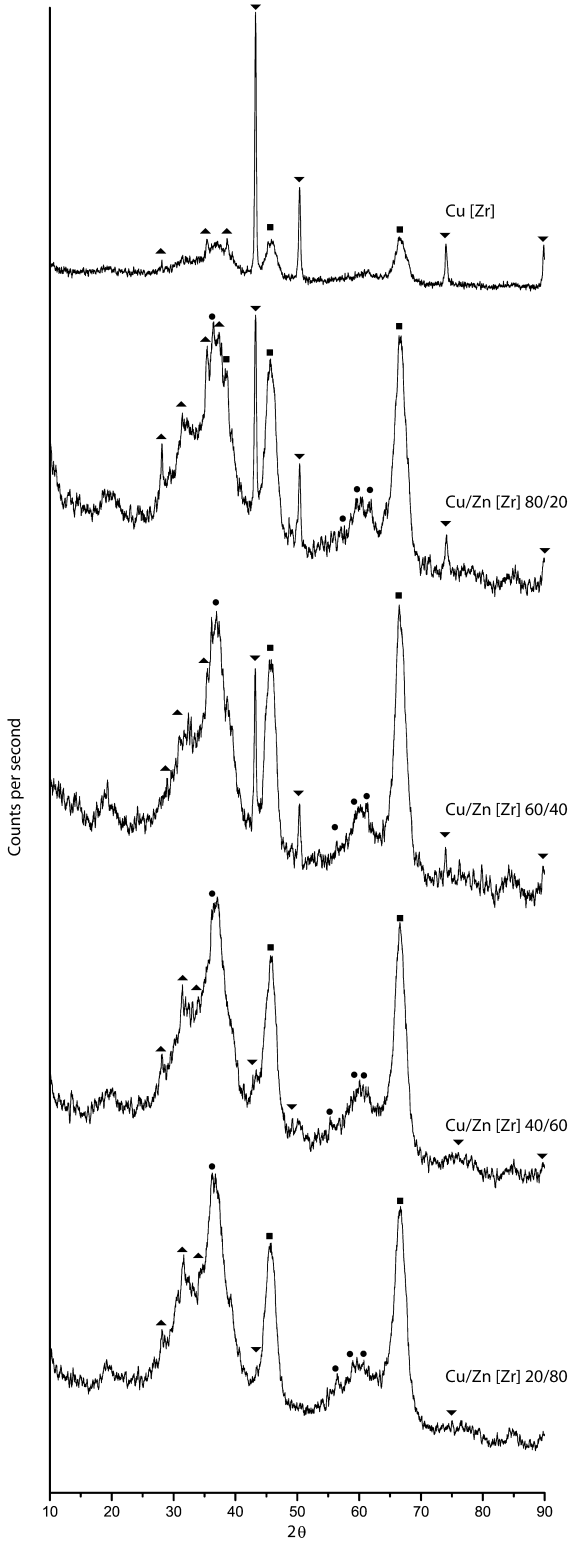

Fig. 12. X-ray diffraction spectra. Cu (▼), γ-Al_2O_3 (■), ZnO (●), ZrO_2 (▲).

for both cases found as metallic copper (Cu^0) indicating that the reduction of the copper oxide (CuO) was effective. Zinc was identified as a separate oxide (ZnO). The zirconium existed in one oxide state (ZrO_2) for all of the doped

Table 6
BET surface area for alumina-supported catalysts

Catalyst Cu/Zn	Surface area (BET) (m^2/g)	Catalyst Cu/Zn [Zr]	Surface area (BET) (m^2/g)
100/0	106	100/0	109
80/20	109	80/20	120
60/40	111	60/40	121
40/60	108	40/60	119
20/80	101	20/80	123
0/100	105		

catalysts. The aluminium oxide was for all cases in the gamma phase.

The specific surface areas obtained from the BET measurements were fairly similar (see Table 6) with the highest area acquired from the zirconium-doped catalyst.

4. Conclusions

Steam reforming of methanol over monolithic catalysts shows great potential for on-board hydrogen generation. The catalyst composition and content of active material greatly affect conversion and carbon dioxide selectivity. The zirconium-doped catalysts were less active with respect to the hydrogen yield, however, they were more selective towards carbon dioxide over the entire temperature interval. The overall best result with respect to hydrogen yield was obtained from the Cu60/Zn40 catalyst with hydrogen concentrations higher than 60% at 210 °C. The Cu60/Zn40 catalyst produced absolute carbon monoxide concentrations below 1% at all temperatures tested in these experiments.

It is important to note that a low-temperature shift step must be implemented prior to the CO clean-up step for catalysts yielding CO concentrations above 1%. Since, the available space in automotive applications is limited, it is highly undesirable to have to install additional clean-up units in the vehicle. Complete methanol conversion is not obtained for any of the catalysts tested in the experiments and, thus the amount of catalyst used limits the reaction.

Acknowledgements

The authors gratefully acknowledge financial support from Volvo Technological Development Corporation, the Swedish National Energy Administration and KTH-Royal Institute of Technology.

References

[1] T.J. Schmidt, H.A. Gasteiger, R.J. Behm, J. Electrochem. Soc. 146 (1999) 1296–1304.
[2] L.J. Pettersson, R. Westerholm, Int. J. Hydrogen Energy 26 (2001) 243–264.
[3] J. Agrell, B. Lindström, L.J. Pettersson, S.G. Järås, Catalysis 16 (2001), in press.
[4] L. Pettersson, K. Sjöström, Combust. Sci. Technol. 80 (1991) 265–303.
[5] M.L. Cubeiro, J.L.G. Fierro, Appl. Catal. A 168 (1998) 307–322.
[6] S. Velu, K. Suzuki, T. Osaki, Catal. Lett. 62 (1999) 159–167.
[7] J. Agrell, K. Hasselbo, K. Jansson, S.G. Järås, M. Boutonnet, Appl. Catal. A 211 (2001) 239–250.
[8] J. Larminie, A. Dicks, Fuel Cell Systems Explained, Wiley, Chichester, UK, 2000.
[9] J.C. Amphlett, R.F. Mann, B.A. Peppley, D.M. Stokes, in: Proceedings of the 26th Intersociety Energy Conversion Engineering Conference, Boston, Mass., U.S.A., Aug. 4–9, 1991, pp. 642–649.
[10] J.P. Breen, J.R.H. Ross, Catal. Today. 51 (1999) 521–533.
[11] B.A. Peppley, J.C. Amphlett, L.M. Kearns, R.F. Mann, Appl. Catal. A 179 (1999) 21–29.
[12] L. Lloyd, D.E. Ridler, M.V. Twigg, The water-gas shift reaction, in: M.V. Twigg (Ed.), Catalyst Handbook, Wolfe Publishing, London, 1989, pp. 283–339.
[13] S.H. Oh, R.M. Sinkevitch, J. Catal. 142 (1993) 254–262.
[14] K.C. Taylor, Automobile catalytic converters, in: A. Crucq, A. Frennet (Eds.), Catalysis and Automotive Pollution Control, Elsevier, Amsterdam, 1987, pp. 97–116.
[15] L.L. Hegedus, J.J. Gumbleton, CHEMTECH 10 (1980) 630–642.
[16] S.T. Gulati, Ceramic catalyst supports for gasoline fuel, in: A. Cybulski, J.A. Moulijn (Eds.), Structured Catalysts and Reactors, Marcel Dekker, New York, NY, 1998, pp. 15–58.
[17] R.M. Heck, S. Gulati, R.J. Farrauto, Chem. Eng. J. 82 (2001) 149–156.
[18] T. Vergunst, F. Kapteijn, J.A. Moulijn, Appl. Catal. A 213 (2001) 179–187.
[19] B. Lindström, L.J. Pettersson, Int. J. Hydrogen Energy 26 (2001) 923–933.
[20] B. Lindström, J. Agrell, L.J. Pettersson, Chem. Eng. J., 2001, submitted for publication.